Sensors and Actuators A 272 (2018) 325–333

Contents lists available at ScienceDirect

Sensors and Actuators A: Physical

journal homepage: www.elsevier.com/locate/sna

Conducting interpenetrating polymer network to sense and actuate: Measurements and modeling

Tien Anh Nguyen [a], Chia-Ju Peng [a,c], Kätlin Rohtlaid [b], Cédric Plesse [b], Tran-Minh Giao Nguyen [b], Frédéric Vidal [b], Shih-Jui Chen [c], Luc Chassagne [a], Barthélemy Cagneau [a,*]

[a] Un. de Versailles Saint-Quentin/LISV, 10-12 Av. de l'Europe, 78140 Vélizy, France
[b] Un. de Cergy Pontoise, 5 mail Gay Lussac/LPPI, 95031 Cergy-Pontoise Cedex, France
[c] National Central University, 300 Zhongda Rd., 32001 Taoyuan City, Taiwan

ARTICLE INFO

Article history:
Received 25 May 2017
Received in revised form 8 January 2018
Accepted 31 January 2018
Available online 8 February 2018

Keywords:
Conducting polymers
Soft robotics
Soft sensors

ABSTRACT

This paper deals with conducting interpenetrating polymers networks (C-IPN). This class of polymers enables us to actuate and sense with the same material. It is of great interest when system integration or limited workspace are an issue. The C-IPNs allow for large displacements under low voltages (typically up to 5 V) with a reversible process. In this work, we are mainly interested in the modeling of the polymer because of its particular behavior. Experimental results are provided to better understand the behavior of the C-IPN. Based on these results, analytical functions are derived in order to predict both sensor and actuator voltage outputs with a good correlation regarding experimental data. These functions are required to use and control the C-IPNs for future applications.

1. Introduction

Actuators with integrated sensors to monitor the acting forces and movements are a challenging topic and might be useful for different kind of applications. The main challenge is to propose a single physical system with both sensing and actuating capabilities in reasonable dimensions. For high reliability and precision in micro-assembly [1,2] and micro-robotics [3–5], demand for sensitized actuators continues to rise [6,7]. However, caused by the physical size and the workspace of micro-actuators, the capacities for added sensors are limited. In order to handle and manipulate microscale objects without any damage, the integration of actuators and sensors in a restricted volume may be of primary interest.

Various driving techniques of micro-actuators and micro-grippers have been developed, including piezoelectric actuators [8–10], electrothermal actuators [11–13], electromagnetic actuators [14,15], electrostatic actuators [16], shape memory alloys (SMAs) [1,17,18], and electronic conducting polymers (ECPs) [19–21]. For example, lead zirconate titanate ($Pb(Zr,Ti)O_3$) piezoceramics, commonly called PZT, is one of the most commercialized intelligent materials which makes dimensional change when electric field is applied [22,23]. With innumerous electric dipoles inside the crystal, the material is polarized caused by ion movement and crystal alignment, resulting in the displacement [24,25]. Besides, when stress is applied to piezoelectric material as a sensor, the displacement of dipoles produces an electrical potential by polarization. Piezoelectric actuators have excellent operating bandwidth which is possible to generate large mechanical forces with fast response speed in milliseconds. However, PZT actuators have some limitations since they require high voltages that produce small displacements. Moreover, PZT actuators are brittle because of the structure of ceramic and are thus subject to rigidity and fragility issues [26,27].

Active polymers which perform size or shape change when exposed to electrical stimulation are called EAPs, producing usable mechanical work. Because of their mechanical behaviors, EAPs are so-called "artificial muscle", attracting attention in many applications and disciplines. According to the mechanism of actuation, EAPs are broadly classified into electronic (field-activated) EAPs and ionic EAPs. Electronic EAPs include dielectric EAP, ferroelectric polymer, and electrostrictive graft elastomer, which are often dry materials and driven by high electrical field and Coulomb forces; Ionic EAPs include electronic conducting polymer (ECP), ionic polymer metal composite (IPMC), and ionic polymer gels, whose mechanical responses are related to diffusion or mobility of ions [28–30]. Compared with piezoelectric ceramics, ECPs

* Corresponding author.
E-mail address: barthelemy.cagneau@uvsq.fr (B. Cagneau).

https://doi.org/10.1016/j.sna.2018.01.067
0924-4247/

have the advantage of the specific properties of polymers such as lightness, flexibility, stretchiness and miniaturization [28]. ECP is a subfamily of electroactive polymers (EAPs), becoming popular in actuating applications because of its related electrochemical reaction [31,32]. They are the most promising because of the advantages: low operating voltage, large deformation capabilities, bio-compatibility, ease of manufacturing and integration with micro electro-mechanical system (MEMS). The studies of ECPs including poly(3,4-ethylenedioxythiophene) (PEDOT) [33,34] and polypyrrole (PPy) [35,36] have been proposed. The oxidation or reduction of ECP makes ions exclude or include from the electrolyte for electroneutrality, resulting in the corresponding dimensional change of ECP [37].

Conducting interpenetrating polymer networks (C-IPNs) exhibit a great potential for use as micro-actuators or micro-grippers with the ability to sense and actuate at the same time. C-IPN consists of two electronic conducting polymers (ECPs) which interpenetrate a solid polymer electrolyte (SPE) between them, demonstrating a pseudo-trilayer ECP/SPE/ECP structure.

With a sandwiched SPE as ionic reservoir instead of traditional electrolyte solvent [38], this pseudo-trilayer device can be electrically actuated under low voltage (<2 V) and in open-air. Ions provided by SPE layer will compensate for the charges created/removed from electrodes and will induce opposite volume variations. The redox reactions taking place within the electrodes will then make the structure to bend reversibly depending on the sign of applied voltage. On the other hand, deformation of the C-IPN due to external stimuli produces an electric potential across two ECP electrodes. The bending of tri-layer device contributes to mechanically induced ion motion between layers and shows the corresponding voltage output. As a consequence, an electric potential is measured and the C-IPN can be used as a mechanical sensor.

C-IPNs that integrate ECP electrodes and SPE have been described with several advantages such as repeatability and compact size. Furthermore, interpenetrating polymer networks are a promising SPE integrated solution, consisting of poly(ethylene oxide) (PEO) and nitrile butadiene rubber (NBR), which reach high performances in terms of flexibility, robustness and conductivity [39,40]. Indeed, it has recently been demonstrated that C-IPN transducers can be electrically actuated in open-air with low fatigue [41,42], and their potential is also promising in terms of actuating frequency [43] and miniaturization [44].

To investigate the sensing and actuating modes of C-IPN as well as control issues, we will focus on the empirical modeling of C-IPN to derive analytical functions of electrical responses. In the sensing mode, the model of the output voltage is required to describe the behavior of C-IPN, especially when dealing with interactions between objects and C-IPN transducers. For example, the grasping force of C-IPN gripper must be monitored to avoid damages on the object or to avoid falling objects. Moreover, because the output force and displacement depend on the working voltage of the C-IPN in actuating mode, another objective is to derive the relationship between the input voltage and, as a consequence, the behavior of the C-IPN with respect to the object for further controlling.

In this study, C-IPNs with both sensing and actuating capabilities are presented. The process of fabrication is briefly described in Section 2. The dimensions of C-IPN in this study are in millimeters (length and width) while the thickness is a few hundreds of micrometers (see Fig. 2). The experimental setups are listed in Section 3, different experiments have been conducted for studying two mode of C-IPN. The electrical behavior of the polymers is then studied and models are proposed as well as experimental results. Section 4 is dedicated to the sensors aspects and the results that concern actuators are presented in Section 5. We also demonstrate that the polymer might be used to detect contacts even when it is used in actuating mode. Experimental results that concern this specific behavior are reported in Section 6.

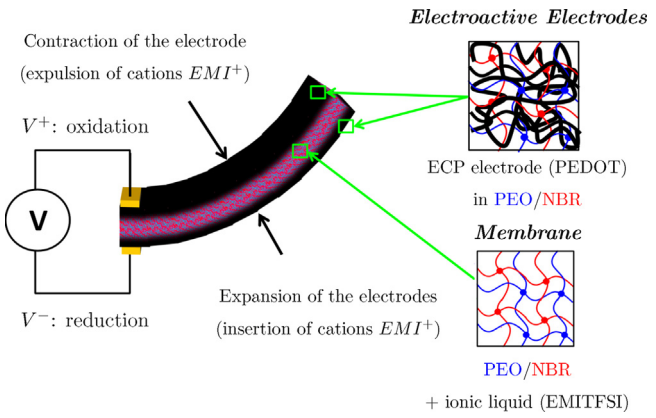

Fig. 1. Schematic representation of the structure and composition of C-IPN used as actuators or/and as sensors.

2. Material and fabrication process

The PEO/NBR IPN films, acting as an ion reservoir in the final product, are synthesized according the procedure described elsewhere [45]. PEO/NBR IPN films are soaked into pure EDOT up to 155 wt% and their surfaces are wiped off with filter paper afterward. The swollen films are then immersed into a $FeCl_3$ aqueous solution (1.5 mol L^{-1}) for 20 h at 22 °C. This step promotes the oxidative polymerization of EDOT into PEDOT within the PEO/NBR IPN, and leads to interpenetrated ECP electrodes. Next, the film is washed several times with methanol until the color disappears completely, i.e. excess of $FeCl_3$ is removed. The conducting material is dried at room temperature under vacuum for 24 h. The edges of the samples are cut off in order to avoid short circuit between PEDOT electrodes. The resulting C-IPN presents a pseudo-trilayer architecture mimicking a classical trilayer device. The material is finally swollen up to saturation ratio (around 150 wt%) in neat electrolyte, 1-ethyl-3-methylimidazolium bis(trifluoromethylsulfonyl) imide (EMITFSI), so as to incorporate ions which are necessary to the redox process of ECP (Fig. 1).

3. Experimental setup

In order to characterize the C-IPN behaviors in sensing mode, a device is used to make a mechanical stimulus to the C-IPN. As shown in Fig. 2, a probe rotates by using a DC motor driven with a microcontroller board. The C-IPN can be bent in both directions (positive and negative deformations, marked as ⊕ and ⊖) depending on the force applied by the probe. The force magnitude and the contact duration is constrained by the rotation angle and the angular velocity of the probe. This experimental system allows the regulation of different parameters used to control the deformation.

Because of the low sensing voltages produced by the deformation (only a few hundreds of microvolts), the amplification of the signal is necessary. An analog amplifier circuit has been developed for the sensing applications, consisting of three successive levels of amplification [46]. To decrease the electronic noise, low-noise operational amplifiers of Analog Device – OP27 are used. The board has two level of non-inverting amplifiers tuned with a gain of 11. The last level is a differential amplifier with a gain of 10, used to compensate for the offset voltage of the transducer that may occur due to residual deformations. Therefore, the signal is amplified with a total gain of 1210. For example, the amplitude of impulse response after amplification is measured at about 0.3 V.

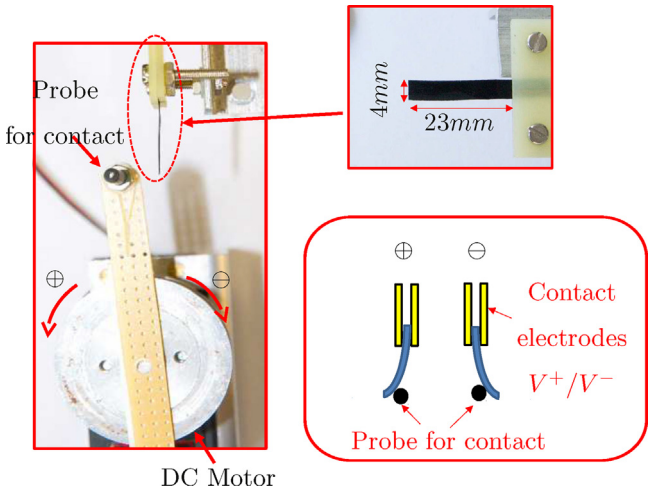

Fig. 2. Forces are applied to the C-IPN with a probe driven by a DC motor. The C-IPN may be deformed in a ⊕ or ⊖ sense.

In this paper, four different experiments are performed to show that a C-IPN has the capabilities of being used as a sensor and a actuator. These experimental setups are presented in Fig. 3. In experiment A (Exp. A) and experiment B (Exp. B), the polymer is used as a sensor. Illustrated in top middle of Fig. 3, the C-IPN is clamped by a two wire-connecting support board, which is linked to the amplifying circuit. When the probe applies a force on the C-IPN transducer, a potential difference is measured between the two electrodes. In experiment C (Exp. C) and experiment D (Exp. D), the C-IPN is actuated by a function generator with/without mechanical contact of the probe.

1. In Exp. A, the C-IPN is bent by the probe starting at t_c and for a duration T_c. Then the DC motor is driven to break the contact at t_r. The C-IPN starts to relax and returns to its initial position, as shown in Fig. 3(A). Exp. A demonstrates a typically mechanical pressure applied on the C-IPN sensor.
2. In Exp. B, the C-IPN is bent by the probe during T_c as same as in Exp. A. However, when the deformation of C-IPN reaches the maximum at t_r, the position of probe is held on by the motor during T_h. The deformation of C-IPN is kept for a duration T_h as illustrated in Fig. 3(B). Exp. B is used to study the response of a deformed C-IPN for a longer duration and a constant position.
3. In Exp. C, the C-IPN is actuated by a function generator and bends toward opposite directions. A resistor is serially linked to prevent from damage of overcurrent. The C-IPN is deflected when voltage is applied as illustrated in Fig. 3(C).
4. In Exp. D, we want to examine the capabilities of the C-IPN to actuate and to sense at the same time. The C-IPN is not only actuated by the generator, but also pressed by the contact of probe as shown in Fig. 3(D). Consequently, a periodic mechanical disturbance produced by DC motor is applied on an actuating C-IPN. This experiment exhibits that C-IPN might be able to detect external forces even when it is used as an actuator.

4. C-IPN as a sensor

In this section, the C-IPN is characterized in sensing mode with the first two experiments A and B. We are interested in the transducer behavior for future applications such as grasping or manipulation. Analytical models are also derived.

4.1. Short deformations

A typical impulse response of C-IPN transducer in experiment A is presented in Fig. 4.

In this paper, we note that such deformation is *short deformation* of C-IPN. When the sensor output reaches the maximum value of $V_{e,max} = 0.3$ V after the bending duration $T_c \approx 5$ s, the DC motor is driven to break the contact. Therefore, the C-IPN starts to relax and returns to its initial position. The impulse response for a short deformation in Fig. 4 is composed of a rising and a falling phase. The rising phase approximately corresponds to a linear increase when the constant force is applied on the C-IPN transducer. The falling

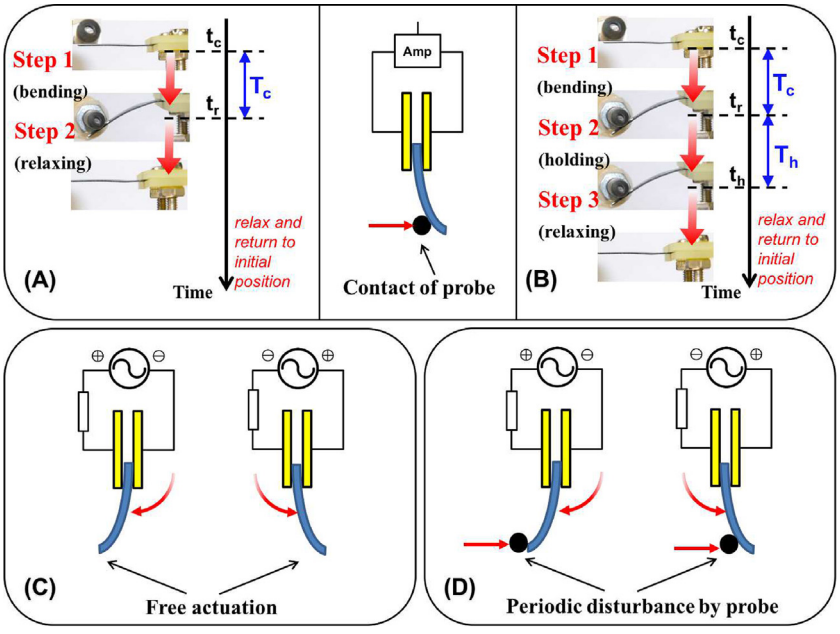

Fig. 3. Schematic diagrams of the 4 experimental setups. The C-IPN in Exp. A and Exp. B is used as a sensor, which is connected to an amplifying circuit. (A) The C-IPN is bent by the probe and the contact duration is T_c. (B) The probe not only moves and bends the C-IPN during T_c as in Exp. A, but also holds its position for a duration T_h. (C) The C-IPN is actuated by a generator without mechanical disturbance. (D) The C-IPN is actuated by the generator and is periodically disturbed by the contact of probe at the same time.

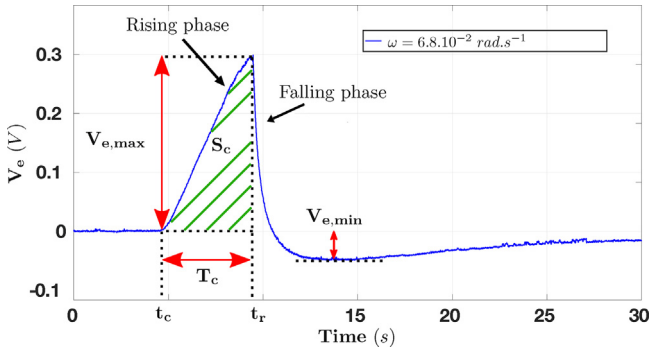

Fig. 4. The C-IPN is deformed for a duration T_c. The contact is then broken.

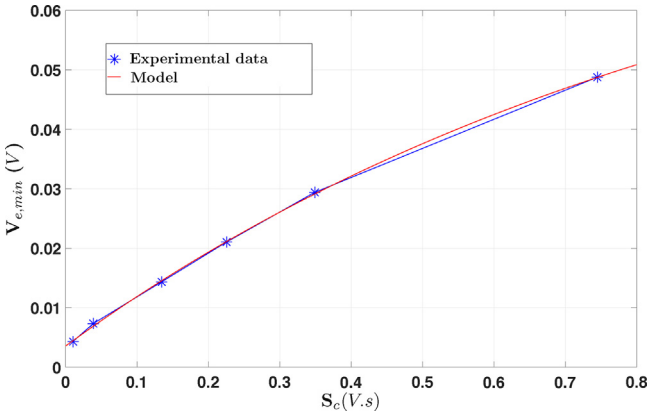

Fig. 6. $V_{e,min}$ as a function of S_c.

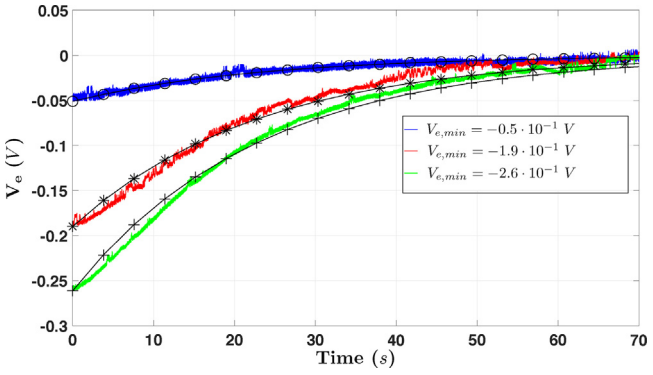

Fig. 7. The sensor output is modeled for different values of $V_{e,min}$. The models are marked with symbols.

phase can be described by an exponential decrease when there is no force applied on the C-IPN anymore.

The rising phase is characterized by two main parameters: the maximum value of impulse response $V_{e,max}$, and the contact duration T_c (the transducer is bent for this duration). The main concern is the effect of T_c regarding the impulse response. Other parameters of the experiments are kept constant. We assume that the magnitude of deformation is constant with the same range of probe positioning for all experiments. T_c is modified by changing the angular velocity of the DC motor. In Fig. 4, $T_c = 5$ s is measured and the angular velocity of DC motor is set to $\omega = 6.8 \cdot 10^{-2}$ rad s^{-1}. It can be noticed that the maximum value of the impulse response $V_{e,max}$ also depends on T_c.

Presented in Fig. 5, despite a constant magnitude of deformation, the maximum output voltage increases when T_c gets higher. In addition, a considerable negative voltage $V_{e,min}$ is clearly observed for low velocities (i.e. higher values of T_c). This phenomenon occurs when the C-IPN is relaxing.

To characterize the effect of T_c on the voltage $V_{e,min}$, the area of rising phase S_c is set as a new parameter computed with Eq. (1):

$$S_c = \int_{t_c}^{t_r} V_e(t)dt \tag{1}$$

By testing different impulse responses corresponding to the values of T_c, $V_{e,min}$ can be represented as a function of S_c based on the fitting model of result, which is shown in Fig. 6. It illustrates the relationship between $V_{e,min}$ and S_c with exponential approximation given by:

$$V_{e,\min}(S_c) = A_0 + B_0 \cdot e^{-C_0 S_c} \tag{2}$$

where $A_0 = 3.6 \cdot 10^{-3}$ V is an offset caused by the initial deformation of the C-IPN transducer which can be easily compensated numerically. $B_0 = -8.3 \cdot 10^{-2}$ V, $C_0 = -1.054$ V^{-1} s^{-1}.

Furthermore, the whole sensor behavior is modeled to predict its output depending on T_c. Fig. 7 shows three different relaxing curves with black lines corresponding to three values of $V_{e,min}$, which fitting the experimental data is given by:

$$V_e(t) = V_{e,\min}\ \ e^{-t/\tau_1} \tag{3}$$

where the time constant is identified as $\tau_1 = 22$ s.

For so-called *short deformations*, the C-IPN stores energy during T_c due to the mechanical strain applied on it. When the contact is

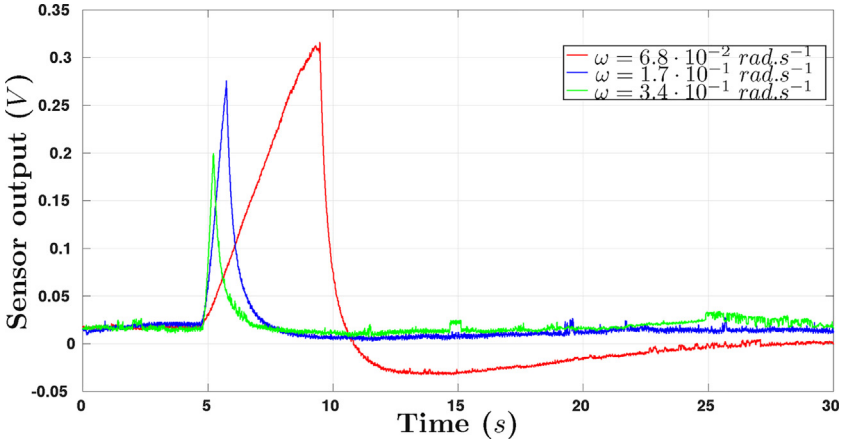

Fig. 5. Responses of the C-IPN to different angular velocities ω of the DC motor.

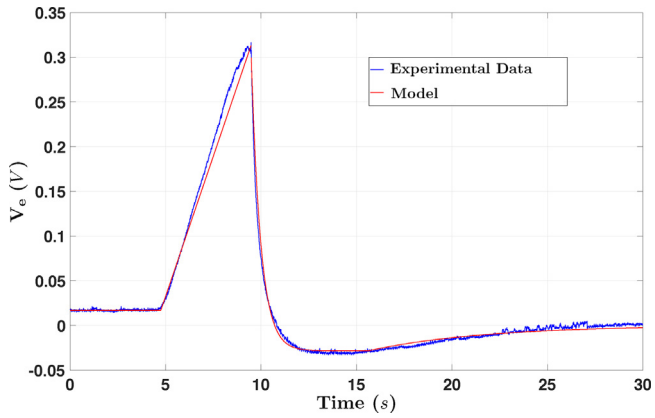

Fig. 8. The full output model of the C-IPN transducer for a short applied with $\omega = 6.8 \cdot 10^{-2}$ rad s^{-1}.

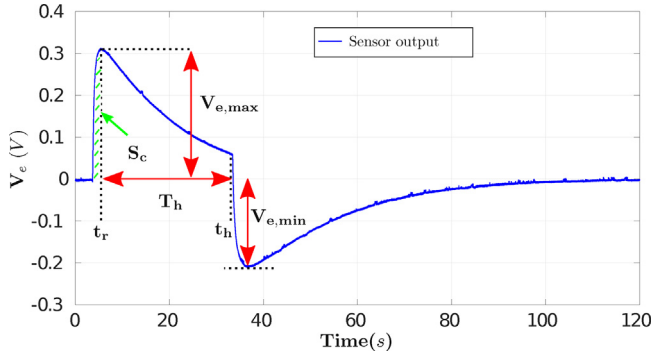

Fig. 9. The C-IPN is in sensing mode. A mechanical constraint is applied for a duration T_h.

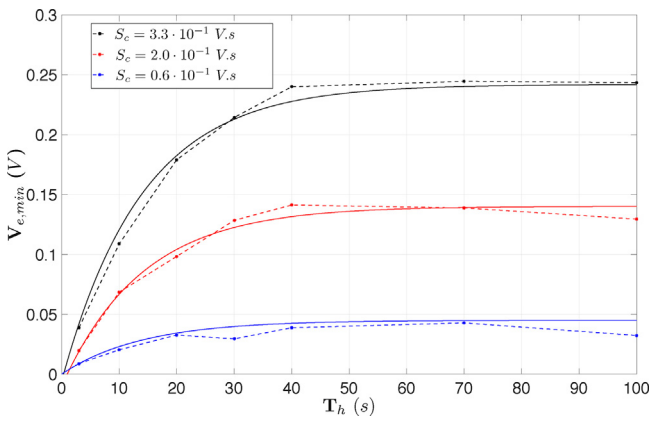

Fig. 10. $V_{e,min}$ as a function of S_c and T_h.

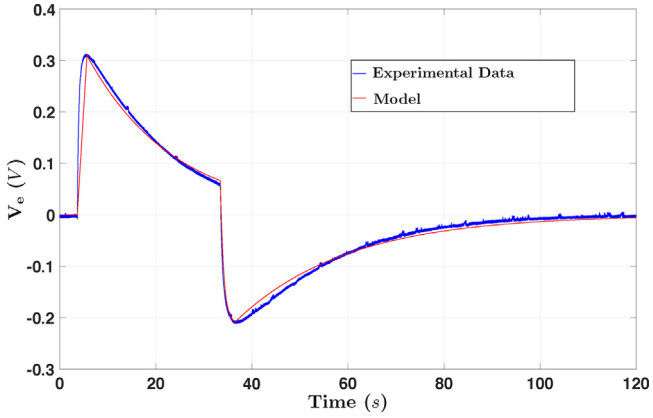

Fig. 11. The full output model of the C-IPN for a long deformation applied with $S_c = 3.3 \cdot 10^{-1}$ V s.

broken, the energy is consumed for returning to its initial state and the residual potential difference $V_{e,min}$ between the two electrodes is then chemically balanced. The full model for the *short deformations* of Exp. A is represented in Fig. 8. Eqs. (2) and (3) are used to model the falling phase. The rising phase is modeled with a linear interpolation and the slope is determined with respect to the angular velocity ω.

4.2. Long deformations

In experiment B, as shown in Fig. 3(B), an initial deformation is applied to the C-IPN, whose behavior before t_r is the same as in Section 4.1. However, the transducer is kept deformed with the same position for a duration $T_h = t_h - t_r$ in this experiment. After t_h, the contact is then broken and a negative peak $V_{e,min}$ is observed. We found that the voltage $V_{e,min}$ could be represented as a function of both S_c and T_h after several experiments. In this paper, we will call this behavior as a *long deformation* (Fig. 9).

The empirical model of $V_{e,min}$ that depends on S_c and T_h is studied. Three values of S_c are selected and the corresponding holding duration is set as $T_h = [3\text{ s}, 10\text{ s}, 20\text{ s}, 30\text{ s}, 40\text{ s}, 70\text{ s}, 100\text{ s}]$. To increase the reliability of estimation, the experimental data is obtained by the average of five trials for each set of $\{S_c, T_h\}$.

As shown in Fig. 10, three experimental curves (blue, red, and black solid lines) illustrate the evolution of $V_{e,min}$ as a function of S_c and T_h. Based on the experimental results, an empirical model is proposed with respect to the holding duration T_h in the range of 3 s to 100 s. For the three values of S_c and the selected values of T_h, this model presents a fair agreement with experimental data. The fitted model is expressed by:

$$V_{e,\min}(S_c, T_h) = A_0 + B_0 \cdot e^{-C_0 \cdot S_c} + D_0 \cdot S_c \cdot (1 - e^{-T_h/\tau_2}) \quad (4)$$

where $D_0 = 0.75$ s^{-1}, $\tau_2 = 14$ s. The value of B_0 and C_0 are the same as in Eq. (2). A_0 depends on the initial state of the polymer, which can be explained by the offset voltage due to some residual deformations and by the heterogeneous environmental condition for the different experiments:

1. $A_0 = 7.8 \cdot 10^{-2}$ V when $S_c = 0.6 \cdot 10^{-1}$ V s
2. $A_0 = 5.7 \cdot 10^{-2}$ V when $S_c = 2.0 \cdot 10^{-1}$ V s
3. $A_0 = 5.3 \cdot 10^{-2}$ V when $S_c = 3.3 \cdot 10^{-1}$ V s

It is interesting to note that, when $T_h = 0$ s, the models expressed in Eqs. (2) and (4) are similar. The additional term that depends on D_0 and τ_2 is required when a holding deformation occurs.

Furthermore, to model the gradually falling phase that occurs during T_h, Eq. (5) is used:

$$V_e(t) = V_{e,\max} \quad e^{-t/\tau_3} \quad (5)$$

where the value $\tau_3 = 18$ s is identified. The full model for the *long deformations* is presented in Fig. 11.

To summarize, the model of C-IPN in sensing mode regarding different types of deformation has been proposed. The whole response of output voltage can be described according to the velocity ω, the bending duration T_c and the holding duration T_h.

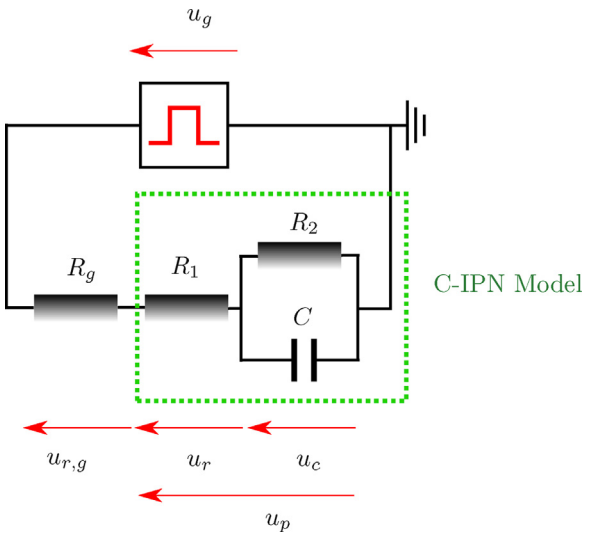

Fig. 12. The C-IPN is modeled with R_1, R_2, C.

5. C-IPN as a actuator

In experiment C, as shown in Fig. 3(C), the C-IPN is used as a actuator. When a voltage is applied, ionic motions contribute to the deformation of the polymer. The electrical model that we propose is necessary to control the C-IPN behavior for future applications.

5.1. Equivalent circuit

The equivalent circuit is proposed in Fig. 12. A generator is used to provide the system with a voltage $u_g(t)$. A resistor R_g is added to prevent from over-current thus the C-IPN will not suffer damage and may be used for a long term. As mentioned above, the C-IPN has two parallel electrodes and electrolyte between them. When a C-IPN is actuated, the electrochemical storage of electricity due to ionic transport between the layers exhibits typical pseudocapacitance [47]. According to Fig. 12, the C-IPN is modeled with a resistor R_1 serially linked to a RC circuit. The capacitor C illustrates the charging behavior of C-IPN through the redox reaction of PEDOT. R_1 represents the resistance of contact and the internal resistance of SPE, which limits the flow of ions in the electrolyte. Besides, a parallel resistor R_2 is included to model a possible leakage current that does not contribute to the actuation [48,49].

5.2. Step response

In this section, the main objective is to derive the analytical voltage $u_p(t)$ of the proposed model. It is indeed useful to control the C-IPN with respect to the input voltage $u_g(t)$. Hereafter, the results are presented for an output that corresponds to a square waveform input. The first set of equations is:

$$\begin{cases} u_g(t) = u_{r,g}(t) + u_r(t) + u_c(t) \\ i(t) = \dfrac{u_c}{R_2} + C \dfrac{du_c(t)}{dt} \end{cases} \tag{6}$$

where $i(t)$ is the current through R_g and R_1. Eq. (6) leads to:

$$u_g(t) = C \cdot (R_1 + R_g) \dfrac{du_c(t)}{dt} + \dfrac{\Sigma R}{R_2} u_c(t) \tag{7}$$

where $\Sigma R = R_1 + R_2 + R_g$.

Let suppose that the initial voltage of the capacitor is $U_c(0) = U_{c,0}$, the Laplace transform (with the Laplace variable p) provides:

$$U_g(p) = C \cdot (R_1 + R_g) \cdot (p \ \ U_c(p) - U_{c,0}) + \dfrac{\Sigma R}{R_2} U_c(p) \tag{8}$$

We are interested in the analytical output of the model. To identify the parameters, $u_g(t)$ is defined as a step of magnitude U_0. As a consequence, the output U_c in Laplace domain is such that:

$$\dfrac{U_0}{p} = C \cdot (R_1 + R_g) \cdot (p \ \ U_c(p) - U_{c,0}) + \dfrac{\Sigma R}{R_2} U_c(p) \tag{9}$$

Eq. (9) can be rewritten as:

$$U_c(p) = \dfrac{U_0 \cdot R_2 \cdot \Sigma R^{-1} + \tau p U_{c,0}}{p(1 + \tau p)} \tag{10}$$

where: $\tau = (R_g + R_1) \cdot R_2 \cdot C \cdot \Sigma R^{-1}$. Applying the inverse Laplace transform, we obtain:

$$u_c(t) = U_0 \cdot R_2 \cdot \Sigma R^{-1} + \left(U_{c,0} - U_0 \cdot R_2 \cdot \Sigma R^{-1}\right) e^{-t/\tau} \tag{11}$$

The voltage applied to the C-IPN is thus computed with Eq. (12):

$$u_p(t) = u_c(t) + R_1 i(t) \tag{12}$$

Combining Eqs. (6) and (12), the output of C-IPN $u_p(t)$ can be presented as:

$$\begin{aligned} u_p(t) = \ & U_0 \dfrac{R_1 + R_2}{\Sigma R} \\ & + \left(1 + \dfrac{R_1}{R_2} - \dfrac{R_1 C}{\tau}\right) \left(U_{c,0} - U_0 \dfrac{R_2}{\Sigma R}\right) e^{-t/\tau} \end{aligned} \tag{13}$$

5.3. Experimental results

The experimental results of actuation in Exp. C with different input voltages are presented in Figs. 13–15. In order to identify the set of parameters (R_1, R_2, C) that appears in Eq. (13), the following conditions are used to deal with experimental data:

$$\begin{cases} u_p(0) & = U_0 \cdot (R_1 + R_2) \cdot \Sigma R^{-1} \\ & \quad + \left(1 + \dfrac{R_1}{R_2} - \dfrac{R_1 C}{\tau}\right) \left(U_{c,0} - U_0 \cdot R_2 \cdot \Sigma R^{-1}\right) \\ \lim\limits_{t \to \infty} u_p(t) & = U_{\text{inf}} = U_0 \cdot (R_1 + R_2) \cdot \Sigma R^{-1} \\ \tau & = (R_g + R_1) \cdot R_2 \cdot C \cdot \Sigma R^{-1} \end{cases} \tag{14}$$

To determine the values of Eq. (14), u_g is defined as a step voltage with a magnitude of ±1.0 V and frequency of 0.1 Hz. The additional resistor R_g is set to 50 Ω. The voltage $u_p(t)$ is measured and presented in Fig. 13.

The system given by Eq. (14) is solved with the experimental values and the parameters of the electrical model can be determined:

$$\begin{cases} R_1 = 42.8 \ \ \Omega \\ R_2 = 50.0 \ \ \Omega \\ C = 6.7 \times 10^{-2} \ \ \text{F} \end{cases} \tag{15}$$

In Fig. 13, the input waveform is presented as well as the simulated electrical model and the experimental results for the output voltage. It appears in Fig. 13 that the electrical model proposed in Fig. 12 is accurate enough to predict the output voltage $u_p(t)$. The numerical values given in Eq. (15) only reflect a set of values based on a mathematical description of the model presented in Fig. 12. The values of R_1 and R_2 are basically chosen to set the DC gain of the transfer function. The value of C, which is quite high, is used to adjust the settling time of the model. Of course, the model may be enhanced with methods such as finite elements but the reason would be to better understand the physical behavior of the C-IPN.

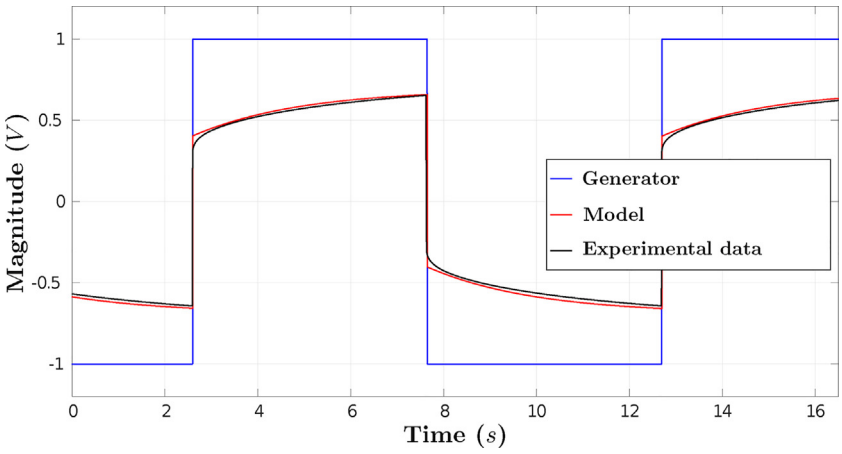

Fig. 13. The C-IPN is actuated with U_g =±1.0 V.

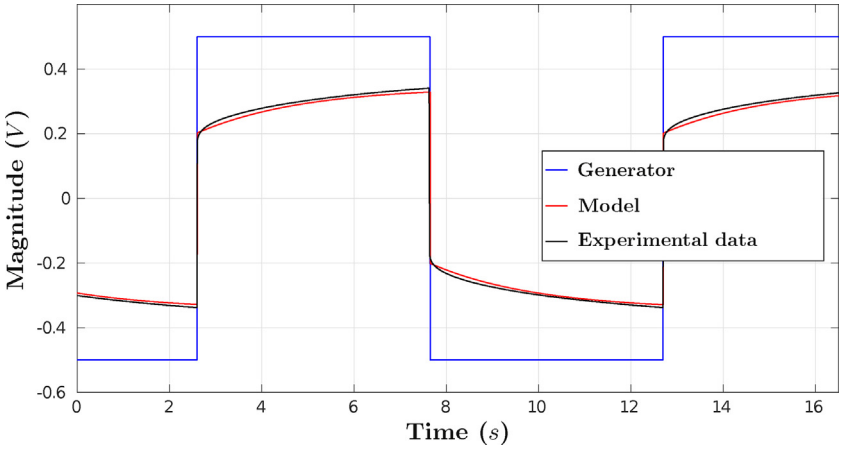

Fig. 14. The C-IPN is actuated with U_g =±0.5 V.

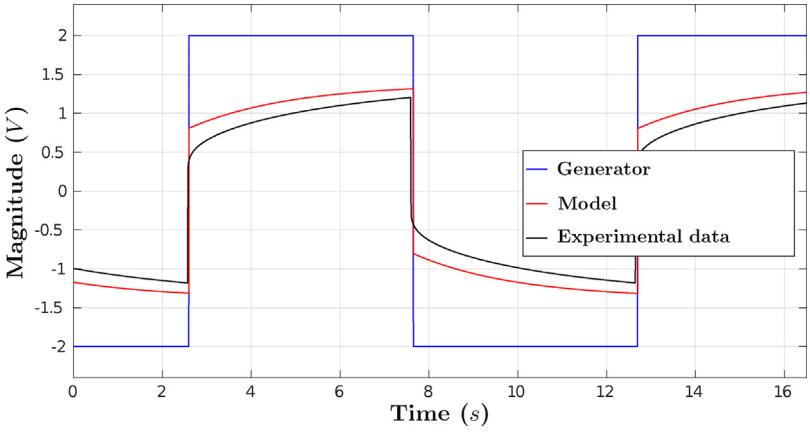

Fig. 15. The C-IPN is actuated with U_g =±2.0 V.

In this paper, we prefer to focus on C-IPN used as tools for applications described in Section 1 and we were only interested in a model which is easy to set.

To validate the model, we have performed the same experiments by changing the input voltage magnitude. It has been set to ±0.5 V and ±2.0 V. The results are presented in Figs. 14 and 15. The experimental results for an input voltage of ±0.5 V are similar to those obtained with ±1.0 V. It means that the electrochemical model is sufficient regarding our needs. The structure proposed in Fig. 12 is easy to study and an analytical function has been derived in Eq. (13). As a consequence, the model can be implemented in real time to predict the C-IPN electrical response.

However, when we set the input voltage to ±2.0 V, the error between the model and experimental data increases. This result demonstrates that the model that we have proposed is not very accurate for high voltages (around 2 V and higher). A solution is to change the model parameters to better fit experimental data. Nevertheless, even if this solution is efficient (results similar to those in

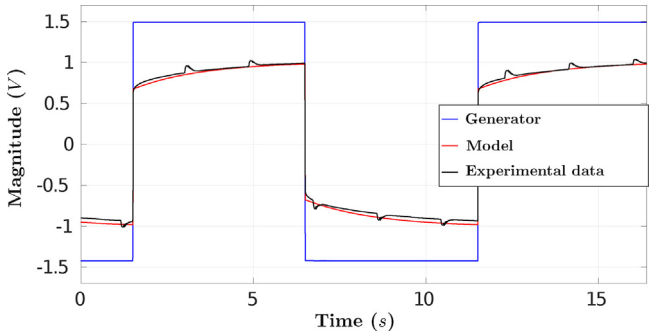

Fig. 16. C-IPN voltage output with mechanical periodic disturbances.

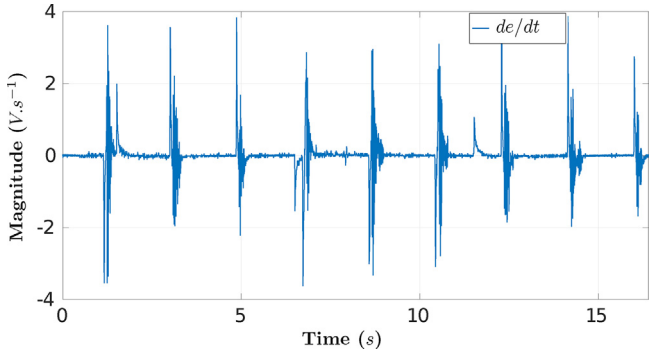

Fig. 17. Derivative of modeling error e to magnify the peaks due to the disturbance.

Figs. 13 and 14 have been obtained), it makes no sense if we want a satisfying solution regarding the physical and mechanical behaviors of the C-IPN. In future work, we will try to derive an unified model over a wide range of input voltages (*i.e.* for voltages higher or equal to 2 V).

6. Actuator with contact detection

In this last experiment (D), the C-IPN is actuated with pulses of magnitude ±1.5 V. However, a periodic mechanical disturbance is applied to the C-IPN presented in Fig. 3 (D). The output voltage is monitored and results are presented in Fig. 16. In this figure, the peaks that correspond to the periodic disturbances can be clearly seen. At our knowledge, it is the first time that a C-IPN is used as a sensor and as a actuator at the same time. It means that this setup could be suitable to perform contact detection while actuating.

The disturbances acting on the C-IPN may be detected by computing the difference between the model derived in previous section and experimental data, which is made with Eq. (16):

$$e(t) = u_m(t) - u_p(t) \tag{16}$$

where $u_p(t)$ stands for experimental measurement and $u_m(t)$ indicates the modeling curve of free actuation. The results are presented in Fig. 17 where the derivative of e is plotted to amplify the peaks. It can be seen that 9 peaks are observable with adequate thresholds as observed in Fig. 16. However, some additional peaks of lower magnitude can be observed. They correspond to the model error when the pulses switch from +1.5 V to −1.5 V and vice-versa. This experiment corresponds to one of the worst case where fast transients occur on the input signal. As a consequence, the model derived in this paper seems sufficient to detect contact for these experimental conditions.

7. Conclusion

In this paper, we have proposed analytical models to control the Conducting Interpenetrating Polymers Network (C-IPN) that we have fabricated. The models are available for both sensing and actuating modes. Moreover, when the C-IPN is used as a sensor, we have shown that the models depend on the deformations applied to it. The behavior of polymers is indeed very different based on the holding durations. We believe that the models which have been developed may be suitable to perform more advanced tasks like object grasping.

Besides experiments at macroscale, we are very interested in the fabrication and the control of C-IPNs at microscale. First material is already available and described in [50]. However, since the size has been drastically reduced, we still need to characterize their electrical behavior and if they are consistent with the models presented in this paper.

Acknowledgement

This work is made possible with the support of the French National Research Agency (ANR) and the project MicroTIP. Katlin Rohtlaid received financial support from the European Union's Horizon 2020 research and innovation program under the Marie Skłodowska-Curie grant agreement No 641822 -MICACT.

References

[1] J. Cecil, D. Vasquez, D. Powell, A review of gripping and manipulation techniques for micro-assembly applications, Int. J. Prod. Res. 43 (4) (2005) 819–828, http://dx.doi.org/10.1080/00207540512331311813.
[2] V. Seidemann, S. Butefisch, S. Buttgenbach, Fabrication and investigation of in-plane compliant SU8 structures for MEMS and their application to micro valves and micro grippers, Sens. Actuators A-Phys. 97–98 (2002) 457–461, http://dx.doi.org/10.1016/s0924-4247(01)00829-9.
[3] J.S. Randhawa, T.G. Leong, N. Bassik, B.R. Benson, M.T. Jochmans, D.H. Gracias, Pick-and-place using chemically actuated microgrippers, J. Am. Chem. Soc. 130 (51) (2008), http://dx.doi.org/10.1021/ja806961p.
[4] M. Gauthier, C. Clevy, P. Kallio, D. Heriban, Micro- and Nanomanipulation Tools, Wiley, 2015, pp. 369–392, book section Industrial Tools for micromanipulation.
[5] K. Han, S.H. Lee, W. Moon, J.S. Park, C.W. Moon, Design and fabrication of the micro-gripper for manipulating the cell, Integr. Ferroelectr. 89 (2007) 77–86, http://dx.doi.org/10.1080/10584580601077591.
[6] J. Park, W. Moon, A hybrid-type micro-gripper with an integrated force sensor, Microsyst. Technol. Micro- Nanosyst.-Inf. Storage Process. Syst. 9 (8) (2003) 511–519, http://dx.doi.org/10.1007/s00542-002-0267-6.
[7] D.H. Kim, B. Kim, H. Kang, Development of a piezoelectric polymer-based sensorized microgripper for microassembly and micromanipulation, Microsyst. Technol.-Micro- Nanosyst.-Inf. Storage Process. Syst. 10 (4) (2004) 275–280, http://dx.doi.org/10.1007/s00542-003-0330-y.
[8] S.K. Nah, Z.W. Zhong, A microgripper using piezoelectric actuation for micro-object manipulation, Sens. Actuators A-Phys. 133 (1) (2007) 218–224, http://dx.doi.org/10.1016/j.sna.2006.03.014.
[9] A.M. El-Sayed, A. Abo-Ismail, M.T. El-Melegy, N.A. Hamzaid, N.A. Abu Osman, Development of a micro-gripper using piezoelectric bimorphs, Sensors 13 (5) (2013) 5826–5840, http://dx.doi.org/10.3390/s130505826.
[10] T. Morita, Miniature piezoelectric motors, Sens. Actuators A-Phys. 103 (3) (2003) 291–300, http://dx.doi.org/10.1016/s0924-4247(02)00405-3.
[11] M. Rakotondrabe, I.A. Ivan, Development and force/position control of a new hybrid thermo-piezoelectric microgripper dedicated to micromanipulation tasks, IEEE Trans. Autom. Sci. Eng. 8 (4) (2011) 824–834, http://dx.doi.org/10.1109/tase.2011.2157683.
[12] Y.Y. Feng, S.J. Chen, P.H. Hsieh, W.T. Chu, Fabrication of an electro-thermal micro-gripper with elliptical cross-sections using silver-nickel composite ink, Sens. Actuators A-Phys. 245 (2016) 106–112, http://dx.doi.org/10.1016/j.sna.2016.04.045.
[13] B. Hoxhold, S. Buttgenbach, Easily manageable, electrothermally actuated silicon micro gripper, Microsyst. Technol.-Micro- Nanosyst.-Inf. Storage Process. Syst. 16 (8–9) (2010) 1609–1617, http://dx.doi.org/10.1007/s00542-010-1040-x.
[14] T.R. Ger, H.T. Huang, W.Y. Chen, M.F. Lai, Magnetically-controllable zigzag structures as cell microgripper, Lab Chip 13 (12) (2013) 2364–2369, http://dx.doi.org/10.1039/c3lc50287b.
[15] S. Yim, E. Gultepe, D.H. Gracias, M. Sitti, Biopsy using a magnetic capsule endoscope carrying, releasing, and retrieving untethered microgrippers, IEEE

Trans. Biomed. Eng. 61 (2) (2014) 513–521, http://dx.doi.org/10.1109/TBME.2013.2283369.
[16] O. Millet, P. Bernardoni, S. Regnier, P. Bidaud, E. Tsitsiris, D. Collard, L. Buchaillot, Electrostatic actuated micro gripper using an amplification mechanism, Sens. Actuators A-Phys. 114 (2–3) (2004) 371–378, http://dx.doi.org/10.1016/j.sna.2003.11.004.
[17] M. Sreekumar, T. Nagarajan, M. Singaperumal, M. Zoppi, R. Molfino, Critical review of current trends in shape memory alloy actuators for intelligent robots, Ind. Robot. Int. J. 34 (4) (2007) 285–294, http://dx.doi.org/10.1108/01439910710749609.
[18] M. Mertmann, E. Hornbogen, Grippers for the micro assembly containing shape memory actuators and sensors, J. De Physique IV 7 (C5) (1997) 621–626, http://dx.doi.org/10.1051/jp4:1997598.
[19] M.Y. Benslimane, H.E. Kiil, M.J. Tryson, Dielectric electro-active polymer push actuators: performance and challenges, Polym. Int. 59 (3) (2010) 415–421, http://dx.doi.org/10.1002/pi.2768.
[20] A. Maziz, C. Plesse, C. Soyer, C. Chevrot, D. Teyssie, E. Cattan, F. Vidal, Demonstrating kHz frequency actuation for conducting polymer microactuators, Adv. Funct. Mater. 24 (30) (2014) 4851–4859, http://dx.doi.org/10.1002/adfm.201400373.
[21] S. Bhattacharya, B. Bepari, S. Bhaumik, IPMC-actuated compliant mechanism-based multifunctional multifinger microgripper, Mech. Des. Struct. Mach. 42 (3) (2014) 312–325, http://dx.doi.org/10.1080/15397734.2014.899912.
[22] W.B. Spillman, J.S. Sirkis, P.T. Gardiner, Smart materials and structures: what are they? Smart Mater. Struct. 5 (3) (1996) 247–254, http://dx.doi.org/10.1088/0964-1726/5/3/002.
[23] T. Suzuki, I. Kanno, J.J. Loverich, H. Kotera, K. Wasa, Characterization of $Pb(Zr,Ti)O_3$ thin films deposited on stainless steel substrates by RF-magnetron sputtering for MEMS applications, Sens. Actuators A: Phys. 125 (2) (2006) 382–386, http://dx.doi.org/10.1016/j.sna.2005.08.010.
[24] A. Ferreira, J. Agnus, N. Chaillet, J.M. Breguet, A smart microrobot on chip: design, identification, and control, IEEE-ASME Trans. Mechatron. 9 (3) (2004) 508–519, http://dx.doi.org/10.1109/tmech.2004.834646.
[25] P. Muralt, Ferroelectric thin films for micro-sensors and actuators: a review, J. Micromech. Microeng. 10 (2) (2000) 136–146, http://dx.doi.org/10.1088/0960-1317/10/2/307.
[26] J. Cecil, D. Powell, D. Vasquez, Assembly and manipulation of micro devices – a state of the art survey, Robot. Comput.-Integr. Manuf. 23 (5) (2007) 580–588, http://dx.doi.org/10.1016/j.rcim.2006.05.010.
[27] A. Dorey, J.H. Moore, Advances in Actuators, Institute of Physics Publishing, Bristol, UK, 1995.
[28] K.J. Kim, S. Tadokoro, Electroactive polymers for robotic applications, Artif. Muscles Sens. (2007).
[29] Y. Bar-Cohen, Q. Zhang, Electroactive polymer actuators and sensors, MRS Bull. 33 (03) (2008) 173–181.
[30] N. Terasawa, I. Takeuchi, H. Matsumoto, K. Mukai, K. Asaka, High performance polymer actuator based on carbon nanotube-ionic liquid gel: effect of ionic liquid, Sens. Actuators B: Chem. 156 (2) (2011) 539–545, http://dx.doi.org/10.1016/j.snb.2010.09.009.
[31] S.A. Wilson, R.P.J. Jourdain, Q. Zhang, R.A. Dorey, C.R. Bowen, M. Willander, Q.U. Wahab, M.A.H. Safaa, O. Nur, E. Quandt, C. Johansson, E. Pagounis, M. Kohl, J. Matovic, B. Samel, W. van der Wijngaart, E.W.H. Jager, D. Carlsson, Z. Djinovic, M. Wegener, C. Moldovan, R. Iosub, E. Abad, M. Wendlandt, C. Rusu, K. Persson, New materials for micro-scale sensors and actuators an engineering review, Mater. Sci. Eng. R-Rep. 56 (1–6) (2007) 1–129, http://dx.doi.org/10.1016/j.mser.2007.03.001.
[32] R.H. Baughman, Conducting polymer artificial muscles, Synth. Metals 78 (3) (1996) 339–353, http://dx.doi.org/10.1016/0379-6779(96)80158-5.
[33] A. Khaldi, C. Plesse, C. Soyer, E. Cattan, F. Vidal, C. Legrand, D. Teyssie, Conducting interpenetrating polymer network sized to fabricate microactuators, Appl. Phys. Lett. 98 (16) (2011) 3, http://dx.doi.org/10.1063/1.3581893.
[34] S. Taccola, F. Greco, B. Mazzolai, V. Mattoli, E.W.H. Jager, Thin film free-standing PEDOT:PSS/SU8 bilayer microactuators, J. Micromech. Microeng. 23 (11) (2013), http://dx.doi.org/10.1088/0960-1317/23/11/117004.
[35] D. Melling, S.A. Wilson, E.W.H. Jager, Controlling the electro-mechanical performance of polypyrrole through 3-and 3,4-methyl substituted copolymers, RSC Adv. 5 (102) (2015) 84153–84163, http://dx.doi.org/10.1039/c5ra15587h.
[36] B. Gaihre, B. Weng, S. Ashraf, G.M. Spinks, P.C. Innis, G.G. Wallace, Microstructures of conducting polymers: patterning and actuation study, Sens. Actuators A-Phys. 197 (2013) 106–110, http://dx.doi.org/10.1016/j.sna.2013.04.008.
[37] E. Smela, Conjugated polymer actuators for biomedical applications, Adv. Mater. 15 (6) (2003) 481–494.
[38] K. Murata, S. Izuchi, Y. Yoshihisa, An overview of the research and development of solid polymer electrolyte batteries, Electrochim. Acta 45 (8–9) (2000) 1501–1508, http://dx.doi.org/10.1016/s0013-4686(99)00365-5.
[39] N. Festin, C. Plesse, P. Pirim, C. Chevrot, F. Vidal, Electro-active interpenetrating polymer networks actuators and strain sensors: fabrication, position control and sensing properties, Sens. Actuators B-Chem. 193 (2014) 82–88, http://dx.doi.org/10.1016/j.snb.2013.11.050.
[40] C. Plesse, A. Khaldi, Q. Wang, E. Cattan, D. Teyssie, C. Chevrot, F. Vidal, Polyethylene oxide–polytetrahydrofurane–PEDOT conducting interpenetrating polymer networks for high speed actuators, Smart Mater. Struct. 20 (12) (2011), http://dx.doi.org/10.1088/0964-1726/20/12/124002.
[41] D. Zhou, G.M. Spinks, G.G. Wallace, C. Tiyapiboonchaiya, D.R. MacFarlane, M. Forsyth, J. Sun, Solid state actuators based on polypyrrole and polymer-in-ionic liquid electrolytes, Electrochim. Acta 48 (14–16) (2003) 2355–2359.
[42] J.D. Madden, D. Rinderknecht, P.A. Anquetil, I.W. Hunter, Creep and cycle life in polypyrrole actuators, Sens. Actuators A: Phys. 133 (1) (2007) 210–217.
[43] Y. Wu, G. Alici, G. Spinks, G. Wallace, Fast trilayer polypyrrole bending actuators for high speed applications, Synth. Metals 156 (16–17) (2006) 1017–1022.
[44] G. Alici, V. Devaud, P. Renaud, G. Spinks, Conducting polymer microactuators operating in air, J. Micromech. Microeng. 19 (2) (2009) 025017.
[45] N. Festin, A. Maziz, C. Plesse, D. Teyssie, C. Chevrot, F. Vidal, Robust solid polymer electrolyte for conducting IPN actuators, Smart Mater. Struct. 22 (10) (2013), http://dx.doi.org/10.1088/0964-1726/22/10/104005.
[46] T.A. Nguyen, L. Chassagne, B. Cagneau, A. Fannir, K. Rohtlaid, T.M.G. Nguyen, C. Plesse, F. Vidal, C.J. Peng, S.J. Chen, An embedded system to control conducting interpenetrating polymer networks actuators, 2016 IEEE Sensors (2016) 1–3, http://dx.doi.org/10.1109/ICSENS.2016.7808965.
[47] Y. Wang, Y. Song, Y. Xia, Electrochemical capacitors: mechanism, materials, systems, characterization and applications, Chem. Soc. Rev. 45 (21) (2016) 5925–5950, http://dx.doi.org/10.1039/C5CS00580A.
[48] J.D. Madden, P.G. Madden, I.W. Hunter, Conducting polymer actuators as engineering materials, Proc. SPIE, vol. 4695 (2002) 176.
[49] K.-H. Kim, S. Tadokoro, Electroactive Polymers for Robotic Applications: Artificial Muscles and Sensors, Springer, 2007, http://dx.doi.org/10.1007/978-1-84628-372-7.
[50] S.E. Takalloo, K. Rohtlaid, N.T. Nguyen, C. Plesse, F. Vidal, E. Cattan, J.D.W. Madden, Design of high-frequency ultrathin trilayer conducting polymer microactuators, Smart Structures, SPIE (2017).

Biography

Barthélemy Cagneau received the Ph.D. degree (2008) in mechanical engineering from the University of Pierre & Marie Curie-Paris 6, Paris (France). After a post-doctoral position in nano-robotics at ISIR (Institut des Systèmes Intelligents et de Robotique, Paris), he became Associate Professor (2009) with the LISV (Laboratoire d'Ingénierie des Systèmes de Versailles, Versailles). His research interests include force control, sensors and robust bilateral couplings for micro- and nano-robotics.